HHS Public Access

Author manuscript

Magn Reson Med. Author manuscript; available in PMC 2019 May 01.

Published in final edited form as:

Magn Reson Med. 2018 May ; 79(5): 2773–2783. doi:10.1002/mrm.26905.

Resting-state functional connectivity in the rat cervical spinal cord at 9.4T

Tung-Lin Wu[1,2,*], **Feng Wang**[1,3], **Arabinda Mishra**[1,3], **George H. Wilson III**[1], **Nellie Byun**[1,3], **Li Min Chen**[1,3], and **John C. Gore**[1,2,3]

[1]Vanderbilt University Institute of Imaging Science, Nashville, TN, United States

[2]Biomedical Engineering, Vanderbilt University, Nashville, TN, United States

[3]Radiology and Radiological Sciences, Vanderbilt University, Nashville, TN, United States

Abstract

Introduction—Numerous studies have adopted rsfMRI methods to infer functional connectivity between cortical regions, but very few have translated them to the spinal cord despite its critical role in the central nervous system. Resting-state functional connectivity between gray matter horns of the spinal cord has previously been shown to be detectable in humans and non-human primates, but it has not previously been reported in rodents.

Methods—rsfMRI of the cervical spinal cord of live anesthetized rats was performed at 9.4T. The quality of the functional images acquired was assessed, and quantitative analyses of functional connectivity in C4–C7 of the spinal cord were derived.

Results—Robust gray matter horn-to-horn connectivity patterns were found that were statistically significant when compared to adjacent control regions. Specifically, dorsal-dorsal and ventral-ventral connectivity measurements were most prominent while ipsilateral dorsal-ventral connectivity was also observed but to a lesser extent. Quantitative evaluation of reproducibility also revealed moderate robustness in the bilateral sensory and motor networks that was weaker in the dorsal-ventral connections.

Conclusions—This study reports the first evidence of resting-state functional circuits within gray matter in the rat spinal cord and verifies their detectability using rsfMRI at 9.4T.

Keywords

fMRI; spinal cord; rat; connectivity

INTRODUCTION

The use of functional magnetic resonance imaging (fMRI) for detecting neural activation has influenced our views of how the brain is organized since the early 1990s. FMRI detects blood oxygenation level dependent (BOLD) signal changes that have been demonstrated to

[*]Corresponding author. Tung-Lin Wu, M.S., Vanderbilt University Institute of Imaging Science, B0104 MC, 1161 21st Ave South, Vanderbilt University, Nashville, TN 37232-2310, Tel: (919) 491-1858, tung-lin.wu@vanderbilt.edu.

reflect underlying neural activity (1,2). Early reports examined only tasked-based studies wherein changes in BOLD signals are interpreted as hemodynamic responses to stimulation (3–6). Later on, the advent of resting-state fMRI (rsfMRI) that identifies patterns of highly correlated low frequency fMRI signals without any task or stimulus has been used to infer functional connectivity between cortical regions (7). Since then, rsfMRI has proven to be a powerful approach to delineate and describe functional circuits, and allows us to assess the manner in which neural systems are intrinsically connected and how they work together to achieve specific functions.

Over the past few decades, numerous studies have used rsfMRI to explore the functional architecture of the brain, but only a handful of studies have translated such techniques to the spinal cord despite its importance serving as a conduit for motor outputs from the brain, peripheral inputs to the brain and as a center for coordinating certain reflexes. This relatively low number of spinal cord fMRI published studies may be attributed to difficulties in obtaining reliable data from the cord because of its small cross sectional area, the augmented influence of physiological noise and magnetic susceptibility issues that arise from surrounding vertebrae and tissues (8). A recent review by Eippert and colleagues provides an overview of data acquisition and processing denoising approaches that have proven useful for spinal cord fMRI (8). Nonetheless, several groups have overcome the challenges of spinal fMRI and have reported task-induced activations in gray matter of the human spinal cord (9–11). Spinal cord injuries in humans have also been demonstrated to exhibit changes in activation detectable with fMRI (reviewed by Stroman et al., 2014 (12))

While task-induced activation and injured patient studies convey valuable information, rsfMRI of the spinal cord potentially could provide a biomarker of the functional integrity of the spine that could be used for clinical diagnosis and prognosis, and the evaluation of therapies, without specific tasks or stimuli, but rsfMRI has been largely unexplored. To our knowledge, reliable rsfMRI in human spinal cord has been demonstrated by only a few other groups to date. Wei et al. applied data-driven independent component analysis (ICA) to describe rsfMRI in the human cervical spinal cord, although the dominant frequency of signal changes was reported to be near the frequency range of the respiratory cycle (13). Two recent studies found distinct dorsal and ventral networks that mirrored spinal cord neuroanatomy, suggesting such observations have a neuronal basis (14,15). We previously reported robust detection of rsfMRI connectivity in human subjects at ultra-high field (7T) using a hypothesis driven region-of-interest (ROI) analysis (16,17). Specifically, Barry et al. found consistent functional connectivity in bilateral motor and sensory networks, while a more recent paper from Eippert et al. confirmed these findings and provided further convincing evidence that spinal cord rsfMRI may be a robust technique for clinical applications (18). Using a similar ROI-based approach, Liu et al. reported that resting-state networks in the upper cervical spinal cord show strong connectivity, and also compared rsfMRI signals across different vertebral levels (19). Harita and Stroman more recently confirmed the presence of spinal cord resting-state BOLD variations and evaluated the contributions of motion and physiological noises to rsfMRI signals in both the brainstem and spinal cord (20).

In order to interpret rsfMRI BOLD signal changes in humans, multi-modal studies in animals may prove valuable, especially if the effects of controlled injuries or interventions can be related to behavior and underlying neural and cellular changes. Animals afford a range of experimental manipulations that are not possible in human subjects (21). Moreover, preclinical imaging at even higher field strengths allows for greater BOLD sensitivity and submillimeter spatial resolution, while injury models allow us to reliably monitor and quantify longitudinal recovery processes in the spinal cord. Previously, we have shown how a non-human primate (NHP) can be used to follow injury-induced disruptions in functional connectivity within and across spinal segments (22). Although NHPs provide a crucial linkage between human and animal data thanks to their high degree of similarity, their use is much more restrictive compared to rodents due to limitations such as handling procedures, costs and management. Moreover, rodents have less inter-subject variability in the brain from an anatomical and functional perspective due to the availability of inbred strains. Thus, we believe imaging of rodent models could provide a robust, cost-effective approach for studying functional organization of the spinal cord and in turn allow a more diverse set of experimental interventions to be investigated.

Significant progress has previously been made towards developing functional imaging of the rat spinal cord, with a focus on detecting stimulus evoked fMRI activation. With early studies indicating that nociceptive information are encoded in the dorsal horns through both temporal and spatial mechanisms (23), using quantitative 2-deoxyglucose mapping, Coghill et al. showed that heat stimulation evoked increased metabolic activity somatotopically within the dorsal horn laminal layers (24). fMRI was subsequently introduced as a tool to evaluate spinal effects caused by noxious stimulation with the injection of formalin (25), as well as electrical stimulation in both the cervical and lumbar spinal cord (26–29). Taking a step further, fMRI in spinal cord was used to detect early stages of diabetic neuropathy, where regions of the lumbar spinal cord presented weaker activation during noxious electrical stimulation when compared to control rats (30). Moreover, Zhao et al. (31) found blood-volume based fMRI in the rat spinal cord to be a robust biomarker of analgesia after the injection of lidocaine. To understand the underlying mechanism of these findings, Lawrence et al. investigated the correlation between neural activation assessed by fMRI and immunohistochemistry by c-fos labeling (32). Overall, these earlier studies demonstrated the utility of fMRI for detecting regions of stimulus-evoked neuronal activity within the spinal cord gray matter.

To date, little is known about the extent to which the spinal cord is expected to demonstrate functional connectivity similar to the brain, nor whether resting-state signal variations correlate with other metrics of activity and connectivity, nor if they are detectable in rodents. Thus, this study reports the first evidence of resting-state networks in the rat spinal cord and verify their detectability at high field. Methods to mitigate some of the challenges of rat spinal cord imaging have been evaluated at 9.4T, which will inform future studies of functional organization of the cord in different conditions.

METHODS

Animal Preparation

Five adult male Sprague-Dawley rats (291±76 grams) were used in this study. Animals were initially anesthetized with 3% isoflurane and underwent endotracheal intubation followed by mechanical ventilation delivering isoflurane in a 1:2 gas mixture of O_2:N_2O. During the scans, ventilation rate was set to 60 breaths/min. End-tidal CO_2 and respiration patterns were continuously monitored. Rectal temperature was also measured and maintained with a thermocouple heating unit at 37°C. Animals were securely placed in a customized bed in the supine position. Before fMRI acquisitions, at least an hour was allocated for physiological stabilization, during which shimming was performed and high resolution anatomical images were acquired. Animals were maintained at a stable anesthesia level (0.9–1.1%) under neuromuscular blockade (vecuronium bromide, 1 mg/kg, i.p.) during functional imaging sessions.

In vivo MRI

All MR images were acquired on a 9.4T Magnex magnet interfaced to a Varian/Agilent spectrometer. A 2-cm diameter transmit-receive radio frequency coil was centered at the C4–C7 region of the rat spinal cord in the iso-center of the magnet. Magnetic field homogeneity was optimized by automatic global shimming and manual fine shimming, followed by local shimming over the spinal cord. In order to locate regions for fMRI data acquisitions, magnetization transfer contrast (MTC) weighted anatomical images were acquired in axial, coronal and sagittal views (Figure 1) using a gradient echo acquisition (TR/TE=200/3 ms, matrix size=128×128, FOV=32×32 mm^2, slice thickness = 3 mm (axial), 0.50 mm (coronal) and 0.75 mm (sagittal), flip angle=35°), which incorporated a Gaussian pre-saturation radio frequency pulse (RF offset=5000 Hz, flip angle=820°, pulse width=12ms).

BOLD images were acquired using a gradient-echo echo-planar imaging (GE-EPI) sequence across five axial slices (TR/TE=500ms/6.70ms, 6 shots, flip angle=35°, resolution=0.33×0.33×3 mm^3, 180 volumes). Similar to the study by Zhao et al. (2009), a relatively short echo time was selected to reduce distortions and signal losses caused by field inhomogenities while the flip angle was adjusted to be approximately equal to the Ernst angle due to the short TR relative to T1 of the spinal cord. Multiple functional runs were obtained for each rat; runs and volumes with excessive motions (> 1.7 mm) and distortions were excluded for subsequent analyses. A total of 21 separate runs from five rats were analyzed for this study.

Data and Statistical Analyses

Resting-state fMRI data were first pre-processed using steps described in Supporting Information. This protocol is a modification of the set of pre-processing steps that our group developed previously for humans and NHPs (17,22). Temporal signal-to-noise (tSNR) maps were constructed by computing the mean of each time series divided by its standard deviation. tSNR was computed as a quality assessment of BOLD images. Averaged time series of the dorsal- and ventral-horn voxels from one slice were displayed and computed after converting raw signal amplitudes to percentage signal BOLD.

Voxel-based correlation maps were calculated using the Pearson's linear correlation coefficient (r) between a seed voxel and all other voxels in the spinal cord. Spinal cord masks that exclude voxels of the CSF were applied. A statistical threshold of $r > 0.4$, $p < 2\times10^{-5}$ was used to depict voxels showing strong correlations within the gray matter horns and white matter. A minimum cluster threshold of 2 voxels was also applied to reduce spurious correlations. This number was determined based on the size of the horns and the actual voxel size to minimize partial volume effects potentially introduced by the linear interpolation from functional to anatomical data (step 2).

An ROI-based correlation analysis was performed using a customized toolbox in *spm12* to summarize functional connectivity between horns of the spinal cord in three slices that correspond to C4/C5, C5/C6, and C6/C7. Our quantitative horn-horn connectivity metrics are similar to those described in two previous papers (17,22). Briefly, *m* individual voxel time series of a horn were correlated with *n* time series of another horn. Subsequently, the maximum of this correlation vector was selected as the metric of functional connectivity between the pair of horns. This was performed for all pairs of ROIs which include the four horns of the spinal cord and two adjacent white matter regions within each slice. Ipsilateral dorsal-ventral correlation values from left and right hemicords were concatenated for group analysis. Similarly for contralateral dorsal-ventral connectivity: left dorsal-right ventral and right dorsal-left ventral measurements were combined. Functional connectivity patterns of interslice ROIs were also evaluated using methods described in our previous publication in NHPs (22). Kong and colleagues have demonstrated the use of data driven methods to separate the spinal cord into different resting-state networks (14). Complementary to such an approach, our method allows us to select regions of the spinal cord based on hypotheses derived from stimulus-driven studies in rats (26,29) and NHPs (22,33). A nonparametric Mann-Whitney-Wilcoxon test was then used to evaluate the differences between different combinations of correlation coefficient pairs. It is also important to note that Bonferroni correction was applied after selecting the voxel that demonstrates the highest correlation; the correction was made to the number of ROI comparisons in group analysis and not voxel-wise at the point of determining the most significant voxel. Lastly, white matter signal was also included as a nuisance signal with separate results presented in Supporting Figure S1.

Lastly, reproducibility and agreement of the connectivity measures were computed within each animal and within each slice. Specifically, fMRI data within each animal were split into two subsets, even and odd runs. Functional connectivity measures from each subset from the same animal were subsequently paired. This was done within each slice for the three slices in the spinal cord. To quantify the degree of reproducibility of spinal cord functional connectivity, Pearson's linear correlation coefficient was computed between the paired runs from the two subsets. Bias and agreement between the two subsets of measures were further evaluated with Bland-Altman plots. These analyses were then repeated with a wider frequency band (0.01–0.16Hz) to investigate the effects of higher frequency (0.1–0.16Hz) on the magnitude and reproducibility of resting-state connectivity measures (r values). Results from data using a wider frequency band are presented in Supporting Figure S2 and Supporting Figure S3.

RESULTS

Quality of BOLD images at the cervical spinal cord

fMRI images were pre-processed in order to minimize motion and physiological noise, and to tease out BOLD signal fluctuations in the spinal cord. Figure 2 presents anatomical images with corresponding BOLD axial images and tSNR maps. A mean tSNR of 36.10±1.69 was computed across all runs in the middle three slices of the spinal cord for the representative rat presented in Figure 2. Figure 3 displays averaged time series of the four horns showing BOLD signal fluctuations similar to those found in humans (16). Functional images are of sufficiently high quality to provide adequate contrast between gray and white matter. In Figure 2, good alignment between anatomical and functional images is also demonstrated with the red and green crosshair pointing to the same left-ventral and right-dorsal horn respectively.

Intrinsic functional connectivity patterns of the rat spinal cord horns

Signal changes to electrical forepaw stimulus have previously been located between C4–C7 segments on ipsilateral dorsal regions. Building upon this finding, we examined ROI-based pair-wise correlation maps of rsfMRI signals in all four spinal horns and white matter regions within these segments of the spinal cord. For example, a seed voxel placed in the dorsal horn results in strong correlation to the corresponding contralateral dorsal horn, and similarly for the ventral horns. The presence of functional connectivity between ipsilateral dorsal-ventral horns is also observed although not consistently across all runs and animals. Number of voxels tested in the spinal cord that exclude voxels of the CSF was on average 132.6 voxels across the middle three slices. Functional connectivity patterns between dorsal-dorsal and ventral-ventral horns were reproducible across animals in this study as shown in Figure 4.

Differential functional connectivity among intraslice ROIs and reproducibility

The strengths of resting-state correlations between different pairs of seeds in the horns within each slice were quantified at the group level. Whisker boxplots of the group mean values and variations of correlation values are presented in Figure 5. Robust correlations are observed between left and right dorsal horns as well as between left and right ventral horns across all four spinal cord segments. For example, mean correlation values of 0.53 and 0.47 were computed for dorsal-dorsal and ventral-ventral connections respectively ($p<0.005$ when compared to white matter controls, Bonferroni corrected) for the C5/C6 segment, although no statistical difference was observed between them. Weaker ipsilateral dorsal and ventral horn connectivity measurements were also observed.

Reproducibility of spinal cord connectivity was quantified with correspondences between odd and even runs from each animal as shown in Figure 6. Qualitatively, data points in correlation plots for dorsal-dorsal (Figure 6A) and ventral-ventral (Figure 6B) connectivity lie predominantly on the diagonal line (slope=1) with correlation values of 0.61 ($p=4.59\times10^{-4}$) and 0.67 ($p=6.71\times10^{-5}$) respectively. In contrast, dorsal-ventral connectivity presents significantly lower correspondence between odd and even runs. Furthermore, visual inspections of the Bland-Altman plots reveal that dorsal-dorsal and ventral-ventral

connectivity measurements present smaller ranges of limits, signifying better agreement between measurements, than those of dorsal-ventral connections. Overall, we found that correlation between spinal cord gray matter horns are connected strongly to each other but with varying strengths; in particular, dorsal-dorsal and ventral-ventral connections are most reproducible in terms of strength and spatial distribution along the cord.

Functional connectivity between inter-slice horns

To quantify how far along the spinal cord the functional connectivity extends, we measured correlation coefficients between ROIs in corresponding horns (e.g., left ventral-to-ventral or left dorsal to dorsal) in three slices that spanned C4–C7 (Figure 7). For both ventral-ventral and dorsal-dorsal connections, we observed that voxels within the seed ROI on the same slice were highly correlated (r~0.9), as expected. As the distance between ROIs was increased to one or two slices away, the correlation values dropped significantly (r~0.2 and r~0.1) between both dorsal and ventral horns. It is also important to note that we have only examined connections between dorsal-dorsal and ventral-ventral horns (connectivity between horns of the right hemi-cord are presented in Supporting Figure S4). Incorporating all possible combinations across segments would not only have made the analysis significantly more complex by vastly increasing the number of comparisons, but also the connectivity between dorsal and ventral horns remains speculative even within the same segment. Overall, our observations indicate that functional connectivity in the rodent spinal cords is spatially constrained across one to two cervical segments.

DISCUSSION AND CONCLUSIONS

Challenges in functional imaging of the rat cervical spinal cord

Imaging the rat cervical spinal cord poses multiple challenges. The small cross-sectional area demands high spatial resolution, while the presence of a relatively thick layer of tissue on the animal's back affects sensitivity. With a 2 cm surface coil at ultra-high field of 9.4T, functional imaging at 0.33×0.33 mm^2 in plane resolution provided adequate resolution with reasonable sensitivity. High contrast-to-noise ratio anatomical MTC weighted images allowed us to make precise image alignments and reproduce results within each animal.

The selection of MRI sequence and BOLD image processing steps were key to providing a sensitive protocol for the detection of resting-state networks in the cervical spinal cord. Zhao et al. previously demonstrated the highest sensitivity of fMRI signals to pain stimulus was achieved using GE-blood volume (BV) weighted images, followed by GE BOLD and spin-echo (SE) BOLD in the cervical rat spinal cord (29). Here, a GE-BOLD sequence was selected which avoids the use of a contrast agent. A set of refined image analysis steps was used that was built upon what had been successful in our previous human and NHP studies (17,22). An independent study evaluated similar key pre-processing steps and was successful at reproducing our previous data, which led to that study's conclusion that spinal cord resting-state connectivity is reliably measurable (18). Our findings support these previous studies as reflected in the robust detection of resting-state functional connectivity in rodents.

A potential major challenge to imaging of the cervical spinal cord compared to the brain is the presence of more pronounced physiological noise caused by respiration and cardiac pulsations. The spinal cord is close to large organs such as the lungs which may cause motion, and may result in shifts in the EPI images in the phase encoding direction and changes in B_0 that can significantly degrade the quality of functional images (34). In addition, artifacts due to systematic signal changes through inflow effects may also be induced. In order to minimize such effects, previous studies have used model-based as well as data driven approaches for physiological corrections (8). Harita and Stroman recently reported that 14% and 2.6% of signal variances in rsfMRI of the human spinal cord can be attributed to cardiac and respiratory sources respectively (20). While model-based methods such as RETROICOR have been shown to improve the specificity of detection in humans (35), our experiences in imaging the spinal cord in well-restrained and mechanically ventilated animals under anesthesia at 9.4T have shown such corrections have minimal effects when included in the pre-processing steps (Supporting Figure S5 and Supporting Table S1). The non-instantaneous slice acquisition of BOLD fMRI data across multiple shots may also render the unsuitability of applying RETORICOR. Specifically, the necessary cardiac and respiratory phases for RETROICOR's Fourier modeling cannot be generated uniquely. Thus, the animals' physiological traces were not recorded in this study to allow such corrections but instead, we 1) synchronized ventilation rate to the acquisition interval, 2) used a data-driven approach for physiological noise correction, CompCor method (36), that derives noise regressors from regions that are unlikely to contain neural signals, and 3) securely positioned the animals in a supine position on a customized holder and bed along with administration of paralytic agent. In Figure 4, we see the majority of the connectivity patterns are focally concentrated in the gray matter horns and not in adjacent white matter. We have also included muscle signals as control regions and regressed them out of the time series of gray matter horns. We therefore conclude that gray matter correlations are unlikely to be driven by spatially correlated physiological noise. Conclusions drawn on the relative importance of physiological correction techniques in fMRI studies should also take into account of the suitability of the applied methods. Further discussion on the effects of physiological noise are included in Supporting Information.

Functional relevance of resting-state connectivity in the spinal cord

It has been widely shown that different brain regions engaged in processing specific external stimuli exhibit strong resting-state functional connectivity (2,22,37–39). For example, our previous study of the SI cortex shows regions that represent different distal finger pads are highly correlated in a resting state in both time and space with underlying synchronized electrophysiological activity and anatomical connections between them (40). This observation was further extended to the spinal cord in NHPs where correlation between stimulus-driven activation patterns and resting-state functional connectivity was observed (22,41). Similarly in rats, forepaw pain stimuli have been shown in previous publications to be reliably located in the dorsal horns (26,29). Our finding that dorsal horns of the spinal cord are highly correlated supports these findings and further indicates baseline functional connectivity between gray matter horns of the spinal cord may be an organizational feature of the central nervous system.

Reliability and reproducibility

Our current analysis suggests a moderate reproducibility of bilateral sensory and motor networks in the spinal cord, while dorsal-ventral functional connections appear to be less robust. Similarly in humans, Barry et al. (2015) reported moderate reproducibility in dorsal-dorsal and ventral-ventral connections (intraclass correlation coefficient (ICC) values: 0.53 to 0.58), while dorsal-ventral networks presented weaker reliability (ICC values: 0.35 to 0.46). In bilateral motor and unilateral sensory networks revealed with ICA, Kong et al. (2014) also found fair reliability in more than half the voxels (ICCs > 0.4), and a quarter of the voxels showed good reliability (ICCs > 0.6). In a pain stimulus evoked study of the rat cervical spinal cord, reproducibility reached up to a cross correlation value of 0.81 ($p=1.1\times10^{-9}$) (29). Despite a greater mean correlation strength in the dorsal-dorsal connection, we observed a higher reproducibility in the ventral-ventral network. This observation is consistent with a recent investigation that explored the robustness of spinal cord rsfMRI signals against variations in the analysis pipeline: the study reported excellent robustness in ventral horn connectivity while dorsal horn connectivity was less robust (18). While ventral-ventral connectivity presented high reproducibility in our study, which may be attributed to the reduced inter-subject variability of rats and imaging at a high field, care must still be taken to interpret these findings. As Barry et al. pointed out, these measurements of reliability are dependent on specific experimental details such as imaging protocols and pre-processing pipelines (16). While a direct comparison of these reproducibility measures across different studies cannot be accurately made, our study found a moderate level of reproducibility in bilateral sensory and motor networks.

Inter-species differences

Spinal cord gray matter horns in rats were observed to be highly correlated in this current study, especially between dorsal-dorsal and ventral-ventral horns. These strongly correlated bilateral motor and sensory networks are consistent with what were observed in recent studies of non-human primates and awake humans (17,22). Specifically, we observed the correlation between dorsal horns to be stronger than between ventral horns, although no statistical differences were found between them. This finding is consistent with healthy NHP controls while human studies have reported mixed results. Barry et al. found a greater ventral-to-ventral connectivity and attributed this to the narrower structure of the dorsal horns – thus, more susceptible to partial volume effects and registration inaccuracies – as well as the presence of larger signal dropout in a few slices. The automated isolation of different laminae within dorsal horns was another possibility (16). A more recent human study of the spinal cord, however, did not observe significant differences between the two pairs (18), similar to what we have found here. As shown in the functional images and tSNR maps (Figure 2 and Supporting Table S2), dorsal horns in rats are relatively wide, and signal dropout is minimal. Our manual selection of the dorsal horns also allows for consistent sampling in the laminae regions of the dorsal horns, and thus the presence of such bias is mitigated. From group analysis boxplots of different studies, specific horn-to-horn functional connectivity patterns within segments appears to vary across different species. For example, the functional connectivity between ventral and dorsal horns has been observed in squirrel monkeys while such connections are still speculative in humans (17,18). Similarly, in rats, ipsilateral dorsal and ventral connectivity was observed to have a weaker correlation

strength but remains statistically significant when compared to control regions. This within hemi-cord connectivity may be associated with sensorimotor functions such as reflexes that may be more pronounced in rodents than in humans. As Chen et al. pointed out, these differences can be associated with the functional organizations of different species (22). The use of more coordinated bilateral behaviors in rats and non-human primates may account for the differences in functional connectivity with humans. The use of anesthesia could also affect the differences with awake human studies. Rodent studies have demonstrated a loss of specificity in cortical regions with elevated anesthesia levels (42,43). However, this appears unlikely at the anesthesia level used in our current study (0.9–1.1%), and reports have shown early cortical regions are less affected by anesthesia. Thus, this effect would most likely be reduced in the downstream spinal cord.

Functional connectivity along the cervical spinal cord

The segmental organization of the spinal cord allows for spatial somatotopic encoding of peripheral information. Our previous study found a bell-shaped spatial correlation profile across five slices that spanned from C4–C7 in ventral horns of NHPs: correlation values dropped from ~r=0.85 to ~r=0.4 and ~r=0.3 as we moved one and two slices away from the ROI seed slice respectively. Overall, functional connectivity across segments was constrained spatially within 2 spinal segments in NHPs (22). Our findings in rodents here indicate a similar trend between ventral-ventral or dorsal-dorsal horns, although larger decreases in correlation values were observed across slices in rodents. A possible explanation is that segments of the rodent spinal cord are thinner than those in NHPs so that a slice thickness of 3 mm may span 1–2 segments in rodents (29) but only 1 segment in NHPs (22,44,45). In humans, Kong et al. have also looked into correlations between segmental levels using an ICA approach, although no correlations between resting-state networks were reported between slices (14). More recently, Liu and colleagues have also reported the presence of significant functional connectivity between vertebral levels and slices in the cervical spinal cord, although the majority of them were still located within vertebral levels as well as within slices. Moreover, amongst the ROI pairs that displayed significant correlations across spinal segments, most of them were also located within 1 segment away from the ROI, similar to what we have found in animal studies (19).

Improvements and future implications

Although we have found robust connectivity between horns of the spinal cord, we can identify several limitations of this study and improvements that could be made. Firstly, our current study has focused mainly on within slice resting-state correlations. While Chen et al. have shown in monkeys the existence of such correlations and how they change before and after injuries, correlation strengths across slices appear to be weaker, consistent with what we have found here in rodents (Figure 7). Similarly, Kong et al. have also investigated correlation between segmental levels using an ICA approach, although no positive nor weak negative correlations were reported between resting-state networks at different spinal cord levels (14). This may be partly the result of the specific pre-processing protocol that was applied on a slice-by-slice basis (i.e. motion correction and regressions) that could reduce correlations between slices but also because correlations fall off between segments. Second, the smoothing with linear interpolation used in this study may have affected these

correlations. However, the likely significance of this appears low as the amount of smoothing introduced was less than a voxel. Care was also taken when selecting ROIs of the horns of the spinal cord (Supporting Figure S6), and correlation maps in Figure 4 present strong correlations between distant voxels. Third, it is important to acknowledge that despite using a refined protocol for imaging the spinal cord, signal drop and distortions in BOLD images are still present especially on slices towards the edge (Figure 2) when compared to anatomical images. Fourth, the use of a 2-cm surface coil limits our field-of-view of the spinal cord. Ideally, measuring how resting-state functional connectivity varies along the entire length of the spinal cord could paint a more complete picture of ascending and descending features with rsfMRI. The use of a coil with greater coverage could be informative but might also introduce increased noise as well as motion artifacts related to respiratory movements. Thus, future developments of imaging techniques would provide us with greater insights into the spinal functional architecture.

Rodents remain to be well suited for preliminary spinal cord injury studies (46), so the use of rsfMRI may be valuable for monitoring their longitudinal recoveries from different manipulations. For example, cervical contusion models in rats have been studied and trends of how they recover behaviorally are well-documented (47). Furthermore, current and investigational drugs as well as regenerative therapy (stem cells) can be introduced to test their effects on the central nervous system and recovery from injury. Another future study will be to extend these techniques to the lumbar spinal cord. Overall, the establishment of rsfMRI in spinal cord in rats may provide us with a robust and cost-effective model to evaluate and develop an effective biomarker for clinical diagnosis, drug development and quantitative monitoring of injuries.

Supplementary Material

Refer to Web version on PubMed Central for supplementary material.

Acknowledgments

The authors gratefully acknowledge Dr. Yue Zhou and Fuxue Xin for their assistance on animal preparation and Ken Wilkens for fine tuning the ventilator. We would also like to thank Dr. Robert L. Barry, Dr. Baxter Rogers and Benjamin Conrad for advices on analysis of spinal functional data. This work was supported by NIH grants NS078680 and NS092961.

References

1. Logothetis NK, Pauls J, Augath M, Trinath T, Oeltermann a. Neurophysiological investigation of the basis of the fMRI signal. Nature. 2001; 412:150–7. [PubMed: 11449264]
2. Fox MD, Raichle ME. Spontaneous fluctuations in brain activity observed with functional magnetic resonance imaging. Nat Rev Neurosci. 2007; 8:700–11. [PubMed: 17704812]
3. Ogawa S, Lee T, Kay A, Tank D. Brain magnetic resonance imaging with contrast dependent on blood oxygenation. Proc Natl Acad Sci U S A. 1990; 87:9868–72. [PubMed: 2124706]
4. Ogawa S, Tank DW, Menon R, Ellermann JM, Kim SG, Merkle H, et al. Intrinsic signal changes accompanying sensory stimulation: functional brain mapping with magnetic resonance imaging. Proc Natl Acad Sci U S A. 1992; 89:5951–5. [PubMed: 1631079]
5. Kwong KK, Belliveau JW, Chesler DA, Goldberg IE, Weisskoff RM, Poncelet BP, et al. Dynamic magnetic resonance imaging of human brain activity during primary sensory stimulation. Proc Natl Acad Sci U S A. 1992; 89:5675–9. [PubMed: 1608978]

6. Bandettini PA, Wong EC, Hinks RS, Tikofsky RS, Hyde JS. Time course EPI of human brain function during task activation. Magn Reson Med. 1992; 25:390–7. [PubMed: 1614324]
7. Biswal B, FZ Y, VM H, JS H. Functional connectivity in the motor cortex of resting human brain using. Magn Reson Med. 1995; 34:537–41. [PubMed: 8524021]
8. Eippert F, Kong Y, Jenkinson M, Tracey I, Brooks JCW. Denoising spinal cord fMRI data: Approaches to acquisition and analysis. Neuroimage. 2016; doi: 10.1016/j.neuroimage.2016.09.065
9. Stroman PW, Ryner LN. Functional MRI of motor and sensory activation in the human spinal cord. Magn Reson Imaging. 2001; 19:27–32. [PubMed: 11295343]
10. Stroman PW, Bosma RL, Tsyben A. Somatotopic arrangement of thermal sensory regions in the healthy human spinal cord determined by means of spinal cord functional MRI. Magn Reson Med. 2012; 68:923–31. [PubMed: 22162154]
11. Kornelsen J, Stroman PW. Detection of the neuronal activity occurring caudal to the site of spinal cord injury that is elicited during lower limb movement tasks. Spinal Cord Off J Int Med Soc Paraplegia. 2007; 45:485–90.
12. Stroman PWW, Wheeler-Kingshott Ca, Bacon M, Schwab JMM, Bosma R, Brooks J, et al. The current state-of-the-art of spinal cord imaging: Applications. Neuroimage. 2014; 84:1082–93. [PubMed: 23859923]
13. Wei P, Li J, Gao F, Ye D, Zhong Q, Liu S. Resting state networks in human cervical spinal cord observed with fMRI. Eur J Appl Physiol. 2010; 108:265–71. [PubMed: 19777254]
14. Kong Y, Eippert F, Beckmann CF, Andersson J, Finsterbusch J, Buchel C, et al. Intrinsically organized resting state networks in the human spinal cord. Proc Natl Acad Sci U S A. 2014; 111:18067–72. [PubMed: 25472845]
15. San Emeterio Nateras O, Yu F, Muir ER, Bazan C, Franklin CG, Li W, et al. Intrinsic Resting-State Functional Connectivity in the Human Spinal Cord at 3.0 T. Radiology. 2016; 279:262–8. [PubMed: 26505923]
16. Barry RL, Smith SA, Dula AN, Gore JC. Resting state functional connectivity in the human spinal cord. Elife. 2014; 2014:1–15.
17. Barry RL, Rogers BP, Smith SA, Gore JC. Reproducibility of resting state spinal cord networks at 7 Tesla. 2015; 23:3708.
18. Eippert F, Kong Y, Winkler AM, Andersson JL, Finsterbusch J, Buchel C, et al. Investigating resting-state functional connectivity in the cervical spinal cord at 3T. bioRxiv. 2016:1–30.
19. Liu X, Zhou F, Li X, Qian W, Cui J, Zhou IY, et al. Organization of the intrinsic functional network in the cervical spinal cord: A resting state functional MRI study. Neuroscience. 2016; 336:30–8. [PubMed: 27590264]
20. Shreyas, Harita, Stroman, PW. Confirmation of resting-state BOLD fluctuations in the human brainstem and spinal cord after identification and removal of physiological noise. Magn Reson Med. 2017; doi: 10.1002/mrm.26606
21. Hutchison RM, Everling S. Monkey in the middle: why non-human primates are needed to bridge the gap in resting-state investigations. Front Neuroanat. 2012; 6:29. [PubMed: 22855672]
22. Chen LM, Mishra A, Yang P-F, Wang F, Gore JC. Injury alters intrinsic functional connectivity within the primate spinal cord. Proc Natl Acad Sci U S A. 2015; 112:5991–6. [PubMed: 25902510]
23. Price, DD. Psychological and neural mechanisms of pain. New York: Raven Press; 1988.
24. Coghill RC, Price DD, Hayes RL, Mayer DJ. Spatial distribution of nociceptive processing in the rat spinal cord. J Neurophysiol. 1991; 65:133–40. [PubMed: 1999727]
25. Porszasz R, Beckmann N, Bruttel K, Urban L, Rudin M. Signal changes in the spinal cord of the rat after injection of formalin into the hindpaw: characterization using functional magnetic resonance imaging. Proc Natl Acad Sci U S A. 1997; 94:5034–9. [PubMed: 9144185]
26. Malisza KL, Stroman PW. Functional imaging of the rat cervical spinal cord. J Magn Reson Imaging. 2002; 16:553–8. [PubMed: 12412032]
27. Malisza KL, Stroman PW, Turner A, Gregorash L, Foniok T, Wright A. Functional MRI of the rat lumbar spinal cord involving painful stimulation and the effect of peripheral joint mobilization. J. Magn. Reson. Imaging. 2003; 18:152–9. [PubMed: 12884326]

28. Zhao F, Williams M, Meng X, Welsh DC, Coimbra A, Crown ED, et al. BOLD and blood volume-weighted fMRI of rat lumbar spinal cord during non-noxious and noxious electrical hindpaw stimulation. Neuroimage. 2008; 40:133–47. [PubMed: 18164630]
29. Zhao F, Williams M, Meng X, Welsh DC, Grachev ID, Hargreaves R, et al. Pain fMRI in rat cervical spinal cord: An echo planar imaging evaluation of sensitivity of BOLD and blood volume-weighted fMRI. Neuroimage. 2009; 44:349–62. [PubMed: 18835453]
30. Malisza KL, Jones C, Gruwel MLH, Foreman D, Fernyhough P, Calcutt NA. Functional magnetic resonance imaging of the spinal cord during sensory stimulation in diabetic rats. J Magn Reson Imaging. 2009; 30:271–6. [PubMed: 19629995]
31. Zhao F, Williams M, Welsh DC, Meng X, Ritter A, Abbadie C, et al. fMRI investigation of the effect of local and systemic lidocaine on noxious electrical stimulation-induced activation in spinal cord. Pain. 2009; 145:110–9. [PubMed: 19560271]
32. Lawrence J, Stroman PW, Bascaramurty S, Jordan LM, Malisza KL. Correlation of functional activation in the rat spinal cord with neuronal activation detected by immunohistochemistry. Neuroimage. 2004; 22:1802–7. [PubMed: 15275936]
33. Yang P-F, Wang F, Chen LM. Differential fMRI Activation Patterns to Noxious Heat and Tactile Stimuli in the Primate Spinal Cord. J Neurosci. 2015; 35:10493–502. [PubMed: 26203144]
34. Raj D, Anderson AW, Gore JC. Respiratory effects in human functional magnetic resonance imaging due to bulk susceptibility changes. Phys Med Biol. 2001; 46:3331–40. [PubMed: 11768509]
35. Glover GH, Li TQ, Ress D. Image-based method for retrospective correction of physiological motion effects in fMRI: RETROICOR. Magn Reson Med. 2000; 44:162–7. [PubMed: 10893535]
36. Behzadi Y, Restom K, Liau J, Liu TT. A component based noise correction method (CompCor) for BOLD and perfusion based fMRI. Neuroimage. 2007; 37:90–101. [PubMed: 17560126]
37. Fox MD, Greicius M. Clinical applications of resting state functional connectivity. Front Syst Neurosci. 2010; 4:19. [PubMed: 20592951]
38. Vincent JL, Patel GH, Fox MD, Snyder AZ, Baker JT, Van Essen DC, et al. Intrinsic functional architecture in the anaesthetized monkey brain. Nature. 2007; 447:83–6. [PubMed: 17476267]
39. Cohen-Adad J, Gauthier CJ, Brooks JCW, Slessarev M, Han J, Fisher JA, et al. BOLD signal responses to controlled hypercapnia in human spinal cord. Neuroimage. 2010; 50:1074–84. [PubMed: 20060914]
40. Wang Z, Chen L, Négyessy L, Friedman R, Mishra A, Gore J, et al. The Relationship of Anatomical and Functional Connectivity to Resting-State Connectivity in Primate Somatosensory Cortex. Neuron. 2013; 78:1116–26. [PubMed: 23791200]
41. Chen LM, Yang P-F, Wang F, Mishra A, Shi Z, Wu R, et al. Biophysical and neural basis of resting state functional connectivity: Evidence from non-human primates. Magn Reson Imaging. 2017; 39:71–81. [PubMed: 28161319]
42. Liu X, Zhu XH, Zhang Y, Chen W. Neural origin of spontaneous hemodynamic fluctuations in rats under burst-suppression anesthesia condition. Cereb Cortex. 2011; 21:374–84. [PubMed: 20530220]
43. Liu X, Zhu XH, Zhang Y, Chen W. The change of functional connectivity specificity in rats under various anesthesia levels and its neural origin. Brain Topogr. 2013; 26:363–77. [PubMed: 23208517]
44. Qi HX, Gharbawie OA, Wynne KW, Kaas JH. Impairment and recovery of hand use after unilateral section of the dorsal columns of the spinal cord in squirrel monkeys. Behav Brain Res. 2013; 252:363–76. [PubMed: 23747607]
45. Florence SL, Wall JT, Kaas JH. Central projections from the skin of the hand in squirrel monkeys. J Comp Neurol. 1991; 311:563–78. [PubMed: 1721925]
46. Cheriyan T, Ryan DJ, Weinreb JH, Cheriyan J, Paul JC, Lafage V, et al. Spinal cord injury models: a review. Spinal Cord. 2014; 52:588–95. [PubMed: 24912546]
47. Pearse DD, Lo TP, Cho KS, Lynch MP, Garg MS, Marcillo aE, et al. Histopathological and behavioral characterization of a novel cervical spinal cord displacement contusion injury in the rat. J Neurotrauma. 2005; 22:680–702. [PubMed: 15941377]

48. Morel P. Gramm: grammar of graphics plotting for Matlab [Data set]. Zenodo. 2016; doi: 10.5281/zenodo.59786

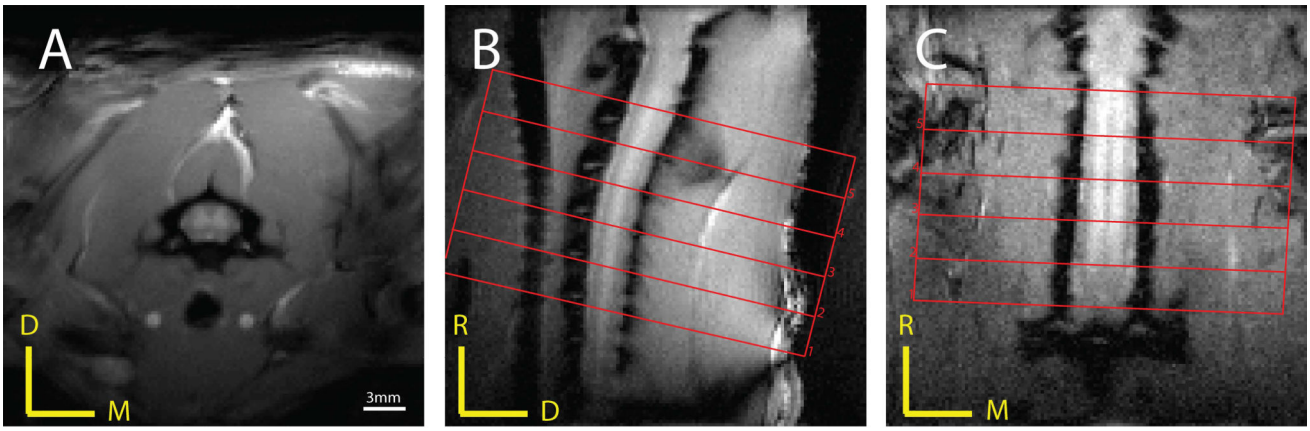

Figure 1.

Magnetization transfer contrast (MTC) weighted anatomical images in three different views. A gradient echo acquisition that incorporated a Gaussian radio frequency saturation pulse was used to obtain (A) axial, (B) coronal and (C) sagittal views of the rat cervical spinal cord with in-plane resolution of 0.25 × 0.25 mm^2 and slice thicknesses of 3 mm, 0.5 mm and 0.75 mm, respectively. Red borders and numbers on the images represent axial slice selections for BOLD images. D: dorsal; M: medial; R: rostral.

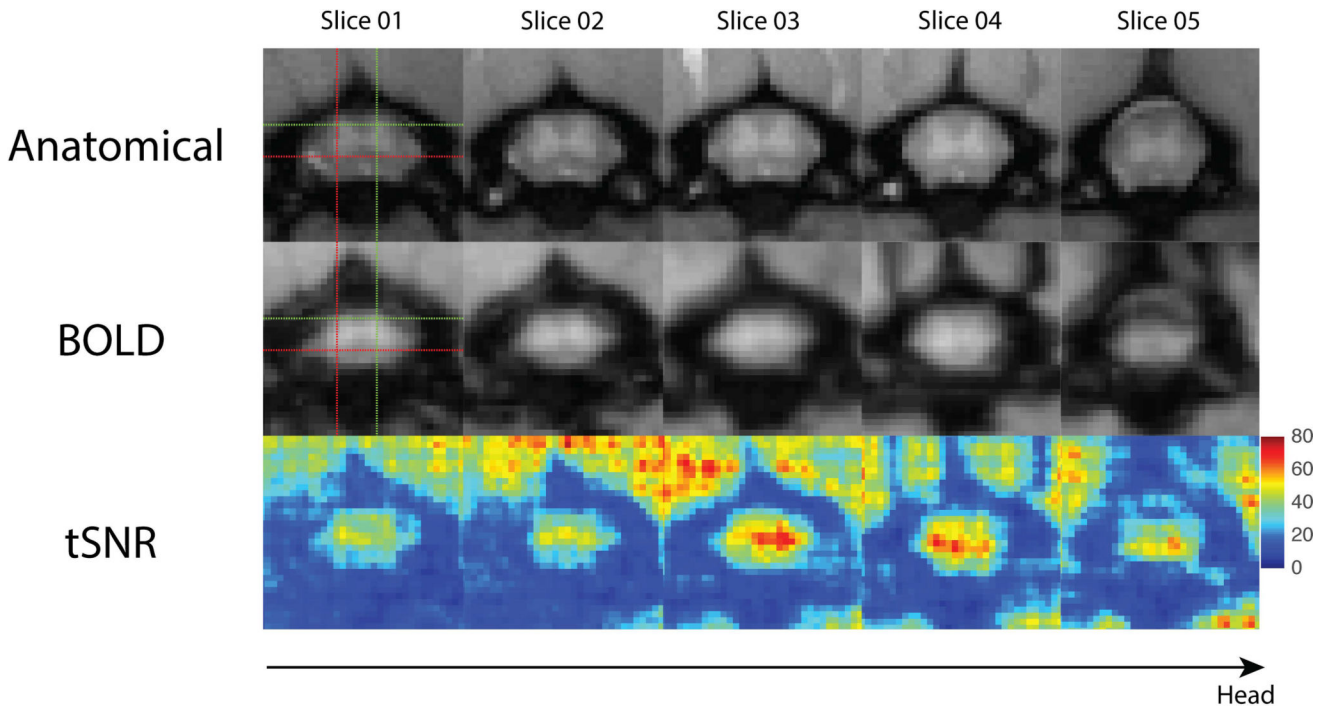

Figure 2.

Anatomical, functional blood oxygenation level dependent (BOLD) and temporal signal-to-noise- ratio (tSNR) maps across five slices. (A) Enlarged views of the cervical spinal cord using magnetization transfer contrast (MTC). Imaging planes of the five slices correspond to the red boxes in Figure 1. (B) Pre-processed functional BOLD images of the same five slices. Goodness of alignments between anatomical and functional images are indicated by the crosshair pointing to the same left ventral horn (red) and right dorsal horn (green). (C) TSNR maps of the functional images presented in B.

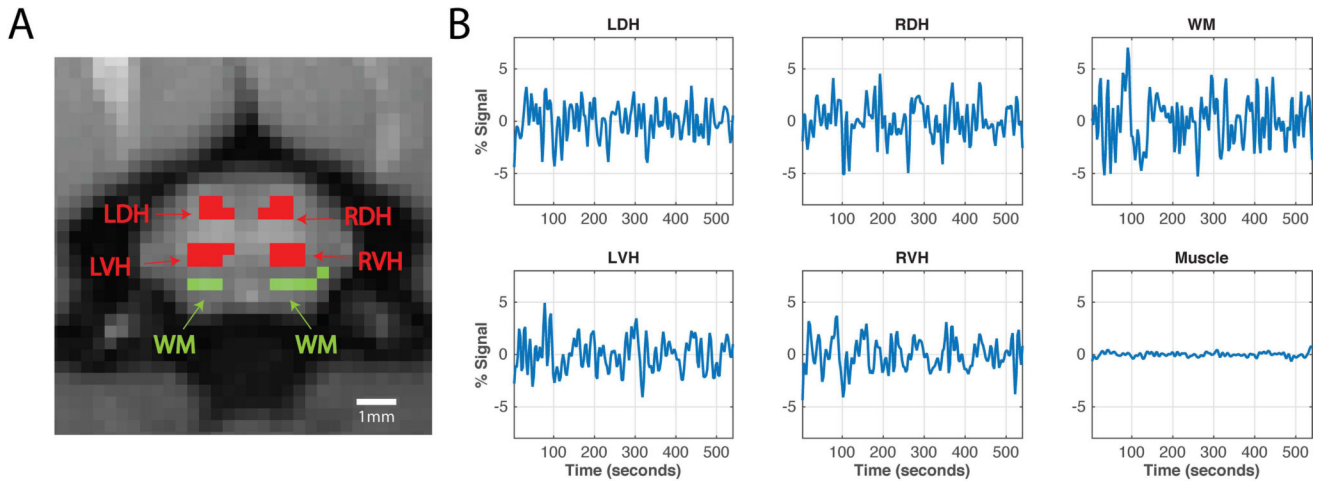

Figure 3.

Horns of the cervical spinal cord, white matter and averaged time series. (A) Anatomical MTC image of the rat cervical spinal cord. Red regions indicate the four horns of the spinal cord – left dorsal horn (LDH), left ventral horn (LVH), right dorsal horn (RDH), and right ventral horn (RVH) – while green regions indicate white matter (WM) voxels that were subsequently used for region-of-interest (ROI) analysis. (B) Averaged BOLD time series of the LDH, RDH, LVH, RVH and WM of the spinal cord, and muscle signal that has been regressed.

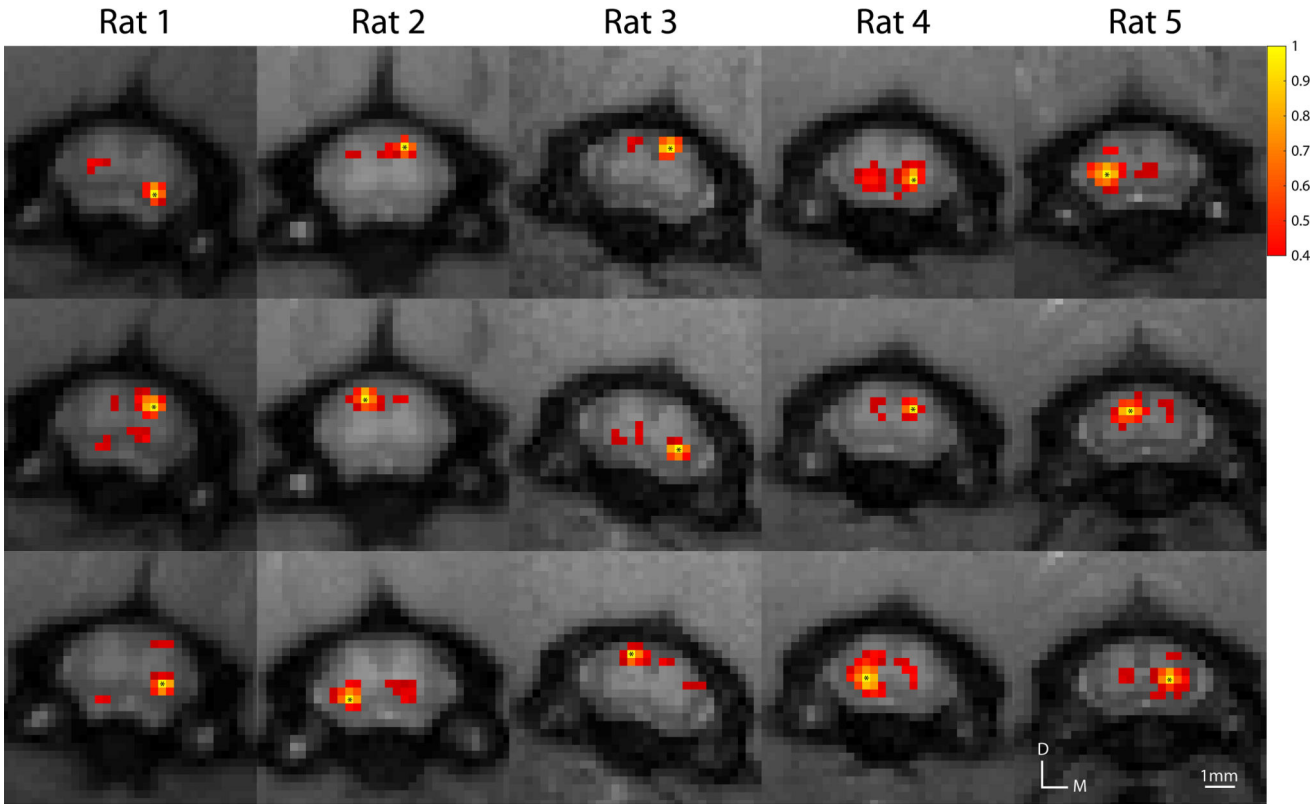

Figure 4.

Examples of within-slice resting-state correlation maps in the cervical spinal cord across all five animals. Correlation maps were thresholded (Pearson's correlation coefficient, $r > 0.4$) and the yellow voxels with asterisks indicate seed voxels. A minimum cluster threshold of 2 voxels was also used to prevent any spurious correlations. D: dorsal; M: medial.

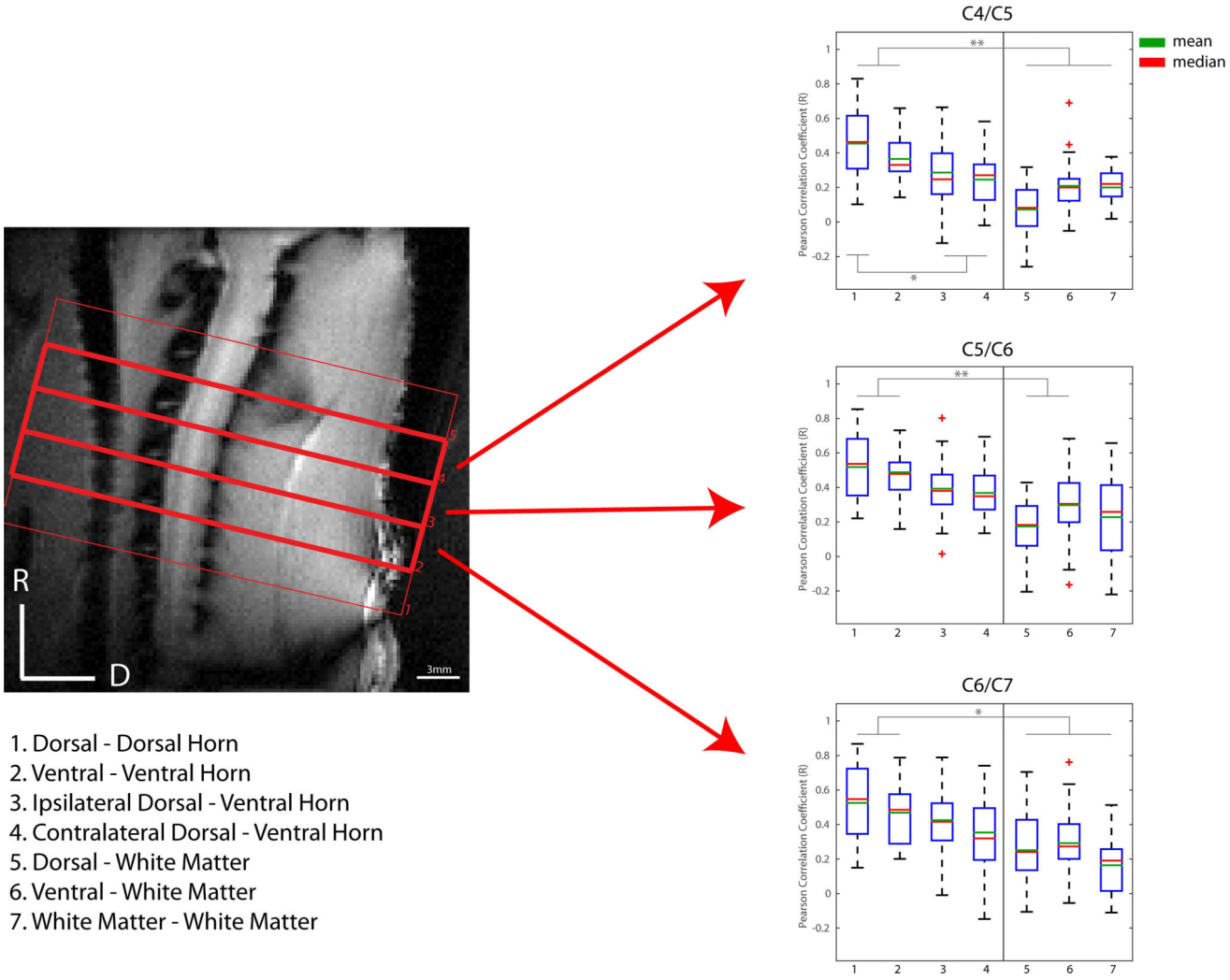

Figure 5.

Group analysis of functional connectivity between spinal cord gray matter horns and "control" white matter regions. (Left) Sagittal MTC image of the rat cervical spinal cord. (Right) Boxplots of correlation strengths between seven ROI pairs in C4/C5 (top), C5/C6 (middle) and C6/C7 (bottom) of the spinal cord. Corresponding slices of each cervical spinal region are indicated by red arrows. *p<0.05, **p<0.005 (non-parametric Mann-Whitney test, Bonferroni corrected). The red crosses represent outlier data points.

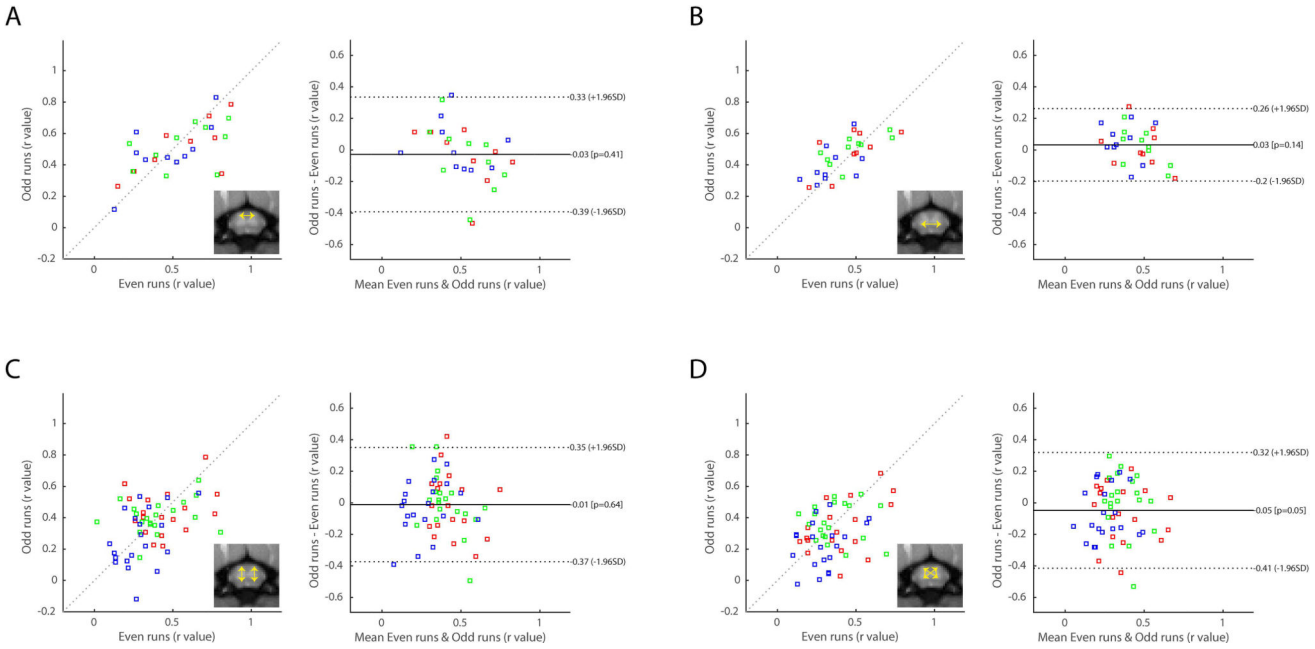

Figure 6.

Reproducibility and agreement of within-slice horn-to-horn functional connectivity. Functional connectivity measurements were divided into two sub-groups that consist of even and odd runs for each animal. (Left of each subplot) Correlation strengths in even runs were then plotted against those in odd runs. To quantitatively measure reproducibility, the cross correlation values (Pearson's coefficient, r) are computed to be 0.61 ($p=4.59\times10^{-4}$) for (A) dorsal-dorsal connectivity, 0.67 ($p=6.71\times10^{-5}$) for (B) ventral-ventral connectivity, 0.25 (p=0.0593) for (C) ipsilateral dorsal-ventral connectivity, and 0.37 (p=0.0044) for (D) contralateral dorsal-ventral connectivity. (Right of each subplot) Bland-Altman plots of horn-to-horn connectivity. Solid lines represent the mean differences between the two subsets, while the dotted lines are 95% limits of agreement. Blue dots denote values from the inferior slice (C4/C5, slice04), green denotes values from the middle slice (C5/C6, slice03), and red dots denote values from the superior slice (C6/C7, slice02).

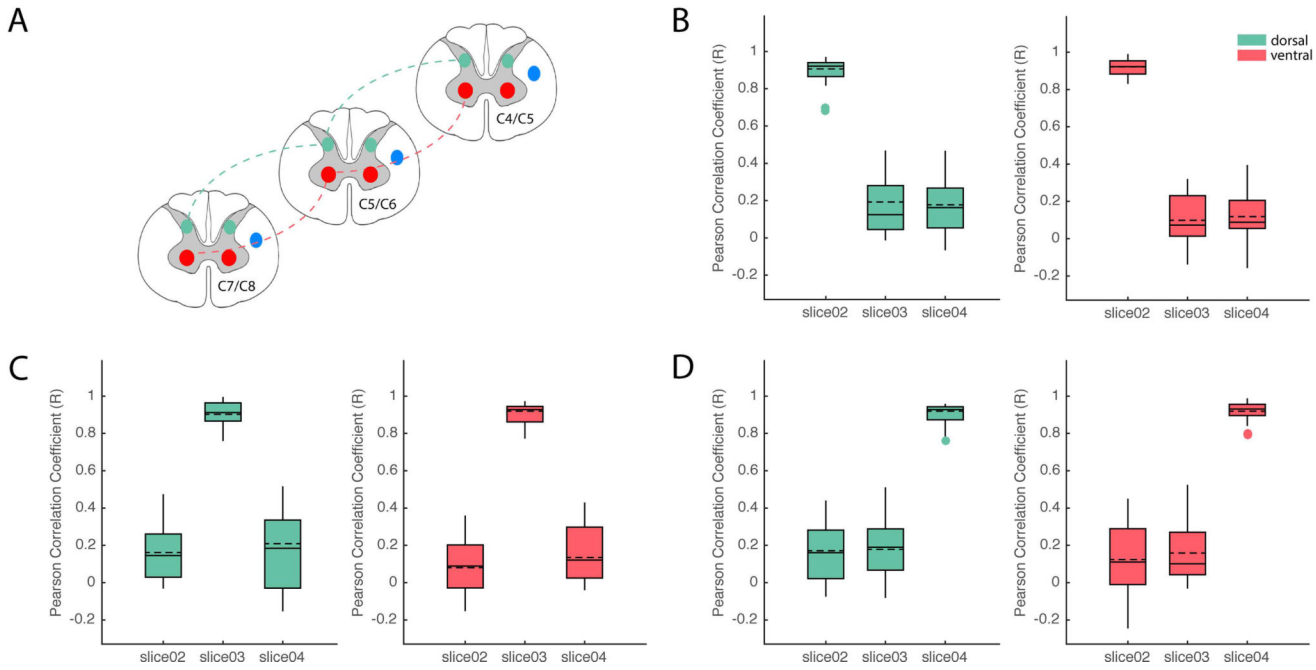

Figure 7.

Group analysis of functional connectivity between spinal cord gray matter horns across different spinal segments. (A) Schematic diagram modified from Chen et al. (22) that illustrates pair-wise correlation analyses with respect to seed ROI in LVH (red lines) and LDH (green lines). (B) Group boxplots of correlation strengths between ROI in slice 2 and those in slices 3 and 4 for both LVH (red shaded boxplots) and LDH (green shaded boxplots). Similarly, correlation strengths were computed and displayed as group whisker boxplots with respect to seeds in slices 3 (C) and 4 (D). Solid and dashed horizontal lines inside each boxplot indicate the median and mean respectively. Shaded boxplots were generated using gramm (48).